energies

MDPI

Article

Oxygen Reduction at PtNi Alloys in Direct Methanol Fuel Cells—Electrode Development and Characterization

Ali Karaca [1], Andreas Glüsen [1], Klaus Wippermann [1], Scott Mauger [2], Ami C. Yang-Neyerlin [2], Steffen Woderich [3], Christoph Gimmler [3], Martin Müller [1,*], Guido Bender [2], Horst Weller [3,4], Marcelo Carmo [1,5,†] and Detlef Stolten [6]

1 Institute of Energy and Climate Research IEK-14: Electrochemical Process Engineering, Forschungszentrum Jülich, 52428 Jülich, Germany
2 National Renewable Energy Laboratory, Golden, CO 80401, USA
3 Center for Applied Nanotechnology CAN, Fraunhofer Institute for Applied Polymer Research IAP, 20146 Hamburg, Germany
4 Department of Chemistry, Institute of Physical Chemistry, University of Hamburg, 20146 Hamburg, Germany
5 Mechanical and Materials Engineering, Queen's University, Kingston, ON K7L 3N6, Canada
6 Chair for Fuel Cells, RWTH Aachen University, 52072 Aachen, Germany
* Correspondence: mar.mueller@fz-juelich.de
† Current address: Nel Hydrogen, Wallingford, CT 06492, USA.

Abstract: Catalyst layers made from novel catalysts must be fabricated in a way that the catalyst can function to its full potential. To characterize a PtNi alloy catalyst for use in the cathode of Direct Methanol Fuel Cells (DMFCs), the effects of the manufacturing technique, ink composition, layer composition, and catalyst loading were here studied in order to reach the maximum performance potential of the catalyst. For a more detailed understanding, beyond the DMFCs performance measurements, we look at the electrochemically active surface area of the catalyst and charge-transfer resistance, as well as the layer quality and ink properties, and relate them to the aspects stated above. As a result, we make catalyst layers with optimized parameters by ultrasonic spray coating that shows the high performance of the catalyst even when containing less Pt than commercial products. Using this approach, we can adjust the catalyst layers to the requirements of DMFCs, hydrogen fuel cells, or polymer electrolyte membrane electrolysis cells.

Keywords: fuel cells; DMFC; supported catalysts; platinum; nickel; alloys; catalyst; ORR; EIS; charge-transfer resistance

Citation: Karaca, A.; Glüsen, A.; Wippermann, K.; Mauger, S.; Yang-Neyerlin, A.C.; Woderich, S.; Gimmler, C.; Müller, M.; Bender, G.; Weller, H.; et al. Oxygen Reduction at PtNi Alloys in Direct Methanol Fuel Cells—Electrode Development and Characterization. *Energies* **2023**, *16*, 1115. https://doi.org/10.3390/en16031115

Academic Editor: Nicu Bizon

Received: 13 December 2022
Revised: 6 January 2023
Accepted: 10 January 2023
Published: 19 January 2023

1. Introduction

The world's energy demand will continually increase, according to the International Energy Agency (IEA) [1]. To meet this demand and limit the environmental impacts, renewable energy technologies will need to make up a larger portion of the total energy production and conversion. This will increase the demand for systems such as electrolyzers and fuel cells. In turn, it will result in a higher demand for catalysts, with platinum being the main option so far for polymer electrolyte membrane (PEM) fuel cell electrodes and DMFC cathodes. Regarding the volatility of platinum's value on the commodity markets and the relatively high price (≈USD 31/g, 20 July 2021 [2]), there will be a need for low-cost, high-performing catalysts that do not depend on natural abundance and volatile stock markets as much. Thus, alternative materials that are abundant and cheap are required. There have been numerous approaches to solve this challenge:

Replace platinum completely by non-precious metals. To our knowledge, that approach has yet not resulted in commercial fuel cell systems that are free of platinum, or with an enhanced activity or stability after using such non-precious catalysts [3–10].

Catalysts with a reduced Pt loading and a higher Pt utilization have been studied for their use as anodic catalysts by different groups [11–13], but in this study we focus on

the oxygen reduction at the cathode. This approach can be split up in several different strategies, which shall be discussed in the following section.

Wang et al. have synthesized the Pt_xNi_{1-x} alloy nanoparticles and characterized them for an oxygen reduction reaction (ORR). Depending on the alloy's composition ($Pt_{75}Ni_{25}$, $Pt_{50}Ni_{50}$, $Pt_{33}Ni_{67}$, and $Pt_{25}Ni_{75}$), there can be an improvement of 3.5 ($Pt_{75}Ni_{25}$) to 4.5 ($Pt_{50}Ni_{50}$) fold in terms of the specific activities (mA cm^{-2}) compared to the Pt nanoparticles supported on carbon [14]. Stamenkovic et al. were able to show that the increased activity of an ORR is a result of weaker oxygen–metal bond interactions when using platinum alloyed with transition metals such as nickel, cobalt, or iron. Pure platinum nanoparticles bind oxygen too strongly and are thus in an oxidized state, which reduces the activity towards a further oxygen reduction. According to the authors, the weaker surface oxide bonds of platinum alloys are a function of a d-band shift of platinum when assuming an atomic platinum layer on the surface and the varying concentration of the alloyed metals in the subsurface layers of the alloy particle.

Based on Density Functional Theory (DFT) calculations, the authors also found that the optimal alloy surface would have a 0.2 eV weaker oxygen binding energy than platinum. Other DFT calculations showed that alloying with cobalt ($Pt_{75}Co_{25}$) or nickel ($Pt_{75}Ni_{25}$) would theoretically result in catalysts with a binding energy in the required range [15]. Antolini et al. have thus tested carbon-supported platinum–nickel ($Pt_{75}Ni_{25}$) and platinum–cobalt ($Pt_{75}Co_{25}$) alloys as anode and cathode electrocatalysts for DMFCs and compared them to platinum nanoparticles. It was shown that $Pt_{75}Ni_{25}$/C on the cathode performed better than the same amount of $Pt_{75}Co_{25}$/C or Pt/C. They also ascribe the higher activities of the nickel-containing alloy to the d-band shift, which was described earlier [16].

Toda et al. described this electronic effect in more detail. They argue that the binding energies at $4d_{3/2}$ or $4d_{5/2}$ orbitals in the Pt skin of PtM (M = 3d-metals such as Ni, Co, and Fe) exhibit positive chemical shifts compared to those of pure platinum by using XPS measurements [17]. The same effect could be observed for some f-orbitals of Pt in the skin layer. They explain this by a lower Fermi level or an increase in the d vacancy in the 5d orbital [17]. Based on these findings and the requirement to reduce the overall platinum loading, it makes sense to alloy platinum with cheap transition metals to reduce the material costs and enhance the catalytic activity. However, beyond the catalyst development, it is critical to understand how to integrate these catalysts into catalyst layers and test them under real fuel cell operations. In this regard, Glüsen et al. have tested the PtNi core shell catalysts produced by the acidic leaching of nickel from PtNi alloys as cathodes for DMFCs [18]. We were able to show that after an extended operation, the bimetallic nanoparticles have improved concerning the performance compared to the initial measurements. This was achieved by operating the cells based on PtNi core shell catalysts containing electrodes over a period of more than 3000 h [9]. Moreover, dealloying of nickel over the course of testing resulted in a Pt shell with the thickness of three atomic layers, which prevents further nickel leaching. Thus, while the catalyst is highly active due to its core shell structure, it is also stable over a long period of time because the further leaching of nickel is prevented [18].

Here, in this paper, we highlight that the incorporation of a new catalyst into the membrane electrode assembly (MEA) is critical to understand the true potential of applied catalyst research. In addition to catalyst properties such as the composition, particle size, structure, and morphology, numerous other aspects can influence the resulting electrode and its overall performance and stability. These aspects can be the coating or transfer method of the electrode onto the membrane, catalyst ink composition (e.g., solvents), electrode thickness, drying procedure, ionomer type, and the ionomer-to-carbon ratio (I/C). As for PEM-based fuel cells, Nafion® is one of the most commonly used ionomers, and the discussion here will be based on that. Subbaraman et al. showed that ionomers inhibit the ORR on Pt-based catalysts. This is due to the absorbing effect of Nafion® on the catalysts' surface, which causes the deactivation of the ORR on Nafion-covered catalysts [19]. Based on this knowledge, it is important to find the best balance between the proton conductivity and catalyst active site availability. There have been numerous approaches which showed

that there is an optimum Nafion® loading [20,21]. For DMFC applications, we have shown in previous works that the optimum of Nafion® loading is also dependent on the operating conditions of the fuel cell [22]. Besides the electrode's ink composition, the ink processing technique and its parameters are crucial for the properties and performance of an MEA. Scheepers et al. showed that the electrode's microstructure is influenced by several factors, one of these being the drying behavior [23]. For instance, if water is enriched during the drying process, it causes the electrodes to crack or delaminate during the film's formation. The delamination of the electrode material has negative effects on further processing, predominantly on the decal transfer step onto the membranes.

While some groups still use commercial electrodes [24] or manual brushing for the electrode's fabrication [25], we here favored the use of the doctor blade coating method as it offers a quick and easy opportunity to produce electrode films with a certain degree of automation in terms of the coating pace and standardization with the slot width [26]. However, one problem cannot be avoided, while a certain part is coated, the rest of the paste remains on the coating table and is pushed further by the squeegee. This will allow the solvents in the paste to evaporate during the film fabrication process, which can change the composition and rheology of the paste. This will eventually influence the catalyst mass loading and properties of the electrode. All these aspects can cause doctor blade coating to be a highly sensitive method to the operating temperature, humidity, and pressure.

Spray deposition is a method that is often used for the fabrication of an electrode [27,28]. While conventional airbrush spraying leads to an inhomogeneous drop size distribution, ultrasonic spraying leads to a homogeneous drop size and therefore a more homogeneous electrode structure as it is fully automated [29–31]. For scaling up the production, other coating techniques would be more favorable in terms of the coating speed and economic feasibility [32–35]. However, to the best of our knowledge, the ultrasonic spraying method provides the best conditions when dealing with the lab scale amounts of the catalyst powders. Moreover, drying phenomena can be neglected to a certain extent because the electrode's fabrication is realized layer-by-layer, whereas a liquid dispersion is sprayed onto the pre-dried previous layer. This is convenient, due to its automation, and a highly reproducible way to produce electrode films for lab-scale batches or even into pilot plants. To take electrodes based on bimetallic catalysts for an oxygen reduction reaction a step further in their development stage, it is necessary to establish techniques for the synthesis of larger amounts than the mg scale. Cathodes must be developed using reproducible techniques that allow for producing both catalytically active thin films for lab applications as well as for small stacks and commercial applications. Thus, in this work, we demonstrate the development and characterization of cathodes used in DMFC operations based on the PtNi (alloy) nanoparticles that were produced in a continuous flow reactor while processing the materials with an automated method employing ultrasonic-spray deposition.

The motivation of this work is to show the potential of bimetallic alloy nanoparticles as a promising alternative for pure Pt nanoparticles. The great impact of this approach is the drastic reduction in precious metal loading and thus the increase in the economic and ecological sustainability of the electrochemical energy conversion in fuel cells in general.

2. Materials and Methods

2.1. Materials, Chemicals, and Catalyst Synthesis

For the preparation of the catalysts nickel(II) bis(acetylacetonate) and platinum(II), bis(acetylacetonate) (98%) was purchased from abcr GmbH, 1,2-hexadecandiol 90%, oleylamine 70%, and oleic acid 90% from Sigma Aldrich, 1,2-dichlorbenzene from Merck, toluene from Honeywell, and ethanol from LoLab. All materials were used as received.

For the electrode paste LQ-1115, Nafion® was used as an ionomer solution (EW 1100, 15% solid content) from Ion Power. Ink formulations were produced with deionized water (18 MΩcm). *n*-propanol (99.7%) was purchased and used as received from Merck. To ensure the reproducibility of the membrane's performance, the Nafion® 115 membrane from Chemours was boiled in hydrogen peroxide solution (3%) for one hour, rinsed in

water three times, and boiled in sulfuric acid (1 mol L^{-1}) for one hour. The treatment with hydrogen peroxide (H_2O_2) removes any organic impurities. With sulfuric acid, cations are replaced by protons and excess reagents are removed by water in each case. After the procedure, the membranes are dried slowly at room temperature (RT) to ensure a quick moistened and a quick start-up. In fact, the membrane manufacturer claims that this process is no longer necessary to do, but we want to be sure that any unexpected results are not due to membrane impurities. Gas diffusion layers (GDL) H2315CX167 were purchased from Freudenberg & Co. KG (Weinheim, Germany). Glass fiber reinforced PTFE films (Reichelt Chemietechnik GmbH & Co. (Heidelberg, Germany)) were used as the decal transfer sheets.

PtNi nanoparticles (4–5 nm) on commercially available Vulcan XC72 were synthesized as described below. The metal-to-carbon ratio was 33% PtNi to 67% carbon. The catalyst production was carried out in a flow synthesis device to ensure the consistent quality of the particles in all the test runs. The flow synthesis was based on a method developed by Ahrenstorff et al. [36]. In a typical synthesis, 4.420 g (25 mmol) of nickel(II) bis(acetylacetonate) and 6.461 g (25 mmol) of 1,2-hexadecanediole were dissolved in a mixture of oleic acid and oleylamine (1:3 molar ratio) and diluted by adding diphenylether, resulting in a stable solution. For the second precursor, 11.799 g (30 mmol) of platinum(II) bis(acetylacetonate) were dissolved in a mixture of oleylamine and 1,2-dichlorbenzene (1:3 volume ratio) and again diluted by adding diphenylether, also resulting in a stable solution. The mixing of the precursors was carried out at 200 °C. To ensure a complete reaction, the mixture was further heated to 240 °C and kept at that temperature for 5 min. The reaction yielded a brownish-black dispersion of the NiPt alloy's nanoparticles. The particles were washed with ethanol for precipitation and dispersed in toluene. The carbon support was added to the dispersion and mixed. Finally, the particles, including the carbon support, were precipitated by adding ethanol one more time.

2.2. Preparation and Fabrication

An overview of the different manufacturing techniques is given by Bee et al. [37]. In this work, all inks were prepared by the following procedures and different compositions have been used to achieve the best electrode layer properties. For the blade, coated electrode inks with an amount of more than 10% catalyst in the solvents were used. Catalyst dispersions with solids content below 5% are required for the ultrasonic spraying of the electrodes:

Blade-coated electrodes. The required amount of catalyst powder was weighed into a syringe. Water was added to avoid ignition. Further i-propanol and the ionomer solution were added. The resulting dispersion was mixed with an ULTRA-TURRAX® (10,000 rpm) for 1 min and treated with an ultrasonic sonotrode while the syringe was cooled in an ice bath. When using this technique, the dispersion was put onto the substrate and by moving a blade with a constant speed and with a constant gap width over the substrate, the ink is distributed homogeneously over the coating area. Since the membrane swells strongly when exposed to solvents and water, in case of electrode manufacturing by blade coating, the decal technique is used, which allows for the dry transfer of the electrode to the membrane, thus avoiding the distortion of the electrode.

Doctor blade coating. The electrode area was removed from a self-adhesive foil using a stamp to create a mask for electrode coating. The foil was then pressed onto a decal transfer sheet. The catalyst ink was filled into a metal frame that was used as a blade to move it over the mask. The electrode's thickness and catalyst loading were controlled by previously defining the foil thickness. The standard foil thickness was 375 µm while the coating velocity was 1 mm s^{-1}. The catalyst loading was controlled by weighing the dry electrodes on the decal foil.

Ultrasonically deposited electrodes. The required amount of catalyst powder was weighed in a laboratory glass bottle, followed by adding water to avoid an ignition. Next, *n*-propanol and the ionomer solution were added. The resulting dispersion was mixed

with an ULTRA-TURRAX® (20,000 rpm) for 1–3 min and treated in an ice-cooled ultrasonic bath for 20 min. For a quality check, the closed glass bottle was rolled with a tube roller. If the particles were visibly attached to the glass wall, the mixing und ultrasonic treatment procedures were repeated until no catalyst particles were visible and the ink looked like a smooth dispersion.

Ultrasonic spray deposition. All ultrasonic spray depositions were conducted with a Sonotek Exacta Coat device. The prepared catalyst inks were filled into a syringe, which was placed in a syringe pump. A movable nozzle is used to distribute the catalyst ink evenly over the coating surface. However, "unlike pressure nozzles, ultrasonic nozzles do not force liquids through a small orifice using high pressure in order to produce a spray. Liquid is fed through the center of a nozzle with a relatively large orifice, without pressure, and is atomized due to ultrasonic vibrations in the nozzle" [38]. A substrate was placed under the spray-head (nozzle) fixed by a vacuum and heated to 80 °C to enable the quick drying of the spray-deposited dispersion. The catalyst ink was then ultrasonically sprayed onto the membrane with a flow rate of 0.3 mL min^{-1} with a 25 kHz accumist nozzle. The catalyst loading was controlled through the number of layers applied and by weighing an electrode coated on a decal foil under the same conditions. The cathodes were deposited directly onto the membrane.

MEA fabrication. Blade-coated cathodes were hot-pressed onto the membrane at 130 °C and 2 kN cm^{-2}. As the focus of this work is the development of cathodes, the authors used standard PtRu anode gas diffusion electrodes (GDEs) produced in-house by slot die coating the catalyst (HiSpec12100) ink onto the Freudenberg gas diffusion layer (GDL) (H2315). The resulting GDE (3.0 mg cm^{-2} PtRu) was hot-pressed (130 °C) onto the membrane with 0.5 kN cm^{-2}. Depending on the cathode ink formulation (i.e., the ionomer content), the cathode GDL was also hot-pressed with 0.5 kN cm^{-2} onto the cathode or just placed onto it manually while assembling the single cell test hardware. The cell geometry was 42 × 42 mm, which corresponds to a geometric surface area of 17.64 cm^2.

2.3. Characterization Methodes

To perform Scanning Electron Microscopy (SEM), all samples were analyzed with a Zeiss, a Gemini Ultra Plus Scanning Electron Microscope, and an Oxford, Ultim Max 100 EDX-Detector.

Cyclic voltammetry (CV) experiments were conducted to determine the electrochemically active surface area (ECSA) of the cathode electrode. To this purpose, the anode was purged with hydrogen (200 mL min^{-1}) as a reversible hydrogen electrode (RHE) and the cathode with nitrogen (200 mL min^{-1}). Once the cell potential reached equilibrium around 0.1 V, the nitrogen flow rate was reduced for the measurement (50 mL min^{-1}). The potential range was 0.05–1.05 V at a scan rate of 20 mV s^{-1}. Each measurement was repeated three times to ensure the reproducibility of the obtained data. All experiments were carried out at room temperature (25 °C).

The peak integrals were used to calculate the electrochemically active surface area (ECSA) using the following equation:

$$ECSA = A_{PI} \cdot \frac{1}{\nu} \cdot \frac{1}{Q} \cdot \frac{1}{M_{PtNi}} \cdot \frac{1}{A_{Geo}} \cdot \frac{1}{10} \quad (1)$$

A_{PI} is the peak integral, ν is the scanning rate, Q is the charge density, M_{PtNi} is the catalyst mass loading, and A_{Geo} is the geometric area of the electrode with the following units:

$$\frac{m^2{}_{Pt}}{g_{Pt}} = (A \cdot V) \cdot \frac{1}{\frac{V}{s}} \cdot \frac{1}{\frac{C}{cm^2{}_{Pt}}} \cdot \frac{1}{\frac{mg_{Pt}}{cm^2{}_{Electrode}}} \cdot \frac{1}{cm^2{}_{Electrode}} \cdot \frac{m^2}{cm^2} \cdot \frac{mg}{g} \quad (2)$$

MEAs with blade-coated electrodes were tested with an electronic load from Höcherl und Hackl (NS506–4). The anode was fed with methanol solution (0.75 mol L^{-1}). The cathode was fed with air at 101 kPa absolute. The air was not preheated or humidified.

Spray-deposited electrodes were tested with a Scribner Associates 850e Fuel Cell Test System. The anode was fed with methanol (0.8 mol L^{-1}). The cathode was fed with air 101 kPa absolute. In both cases, the methanol flow rate was 3.88 mL min^{-1} and the air flow rate was 650 mL min^{-1}. The methanol solution was preheated to 70 °C, which corresponds to the fuel cell operation temperature. The methanol concentration of 0.75–0.8 mol L^{-1} was chosen as it has shown a stable performance over a wide range of current densities in previous studies [39].

Electrochemical impedance spectroscopy (EIS) experiments were carried out using an electrochemical workstation (IM6) from Zahner-Elektrik GmbH & CoKG. In case of galvanostatic measurements, exceeding a total limit of 3 A, a 4-quadrant power potentiostat (PP241) with a maximum current of 40 A was coupled to the electrochemical workstation. The complete cell impedances were measured first. Afterwards, we measured the anode cell impedances by purging the cathode with hydrogen to operate it as a dynamic hydrogen electrode (DHE). The half-cell impedance of the cathode is determined by the subtraction of the complete cell data from the half-cell data of the anode. All measurements were carried out in the potentiostatic mode with a frequency range from 0.1 Hz to 50 kHz. The sinusoidal amplitude was 10 mV at the given DC potential.

All EIS simulations for the data fitting of the calculated cathode EIS spectra were carried out with the Thales simulation program from Zahner-Elektrik GmbH & CoKG (Kronach-Gundelsdorf, Germany). The calculated datasets were fed into the simulation program by using a Hilbert transformation to flatten out the potential artifacts caused by the experimental conditions. Afterwards, the data are fitted by using the equivalent electrical circuit (EEC) chosen beforehand.

3. Results

The synthesized particles consisted of roughly 25% Ni and 75% Pt in a mixed alloy (91 $wt\%_{Pt}$ and 9 $wt\%_{Ni}$); they had a spherical shape and a mean diameter of 3.5 nm. The particles are attached to the carbon carrier (Vulcan XC72) in a ratio of 33.3% Pt_3Ni to 66.7% carbon. Figure 1 shows the even distribution of the catalyst's materials on the carbon carrier.

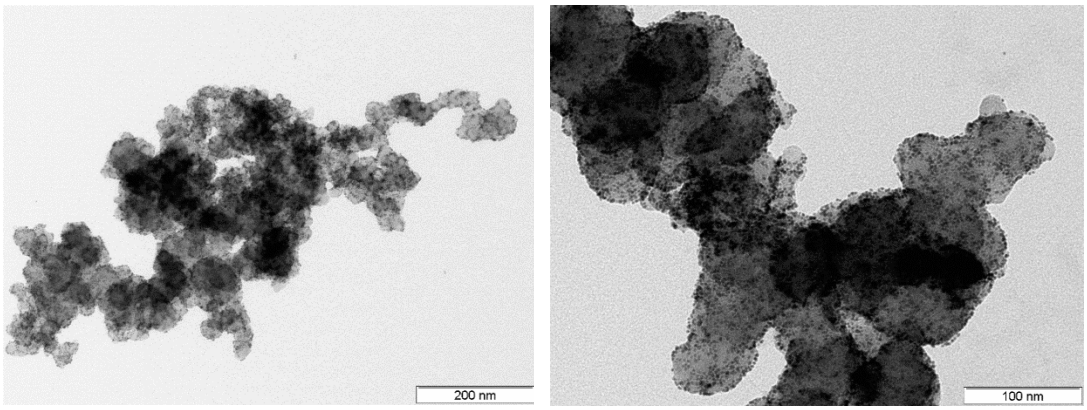

Figure 1. TEM Images of 33.3% PtNi alloys with an average diameter of 3.5 nm distributed on a carbon support (Vulcan XC72) at different magnifications.

3.1. Fabrication Method

Initially, the PtNi catalysts were used to fabricate the catalyst layers by using doctor-blade coating with water/propanol-based inks onto decal substrates. However, all electrode ink mixtures led to electrodes that formed cracks, which eventually resulted in independent flakes that delaminated off the decal transfer sheet prior to the transfer process. This then led to voids in the electrode material which was transferred to the membrane. Figure 2 shows an optical microscopy crack structure analysis after the hot-pressing of an electrode onto a Nafion® 115. Cracks with a width of up to 335 µm were observed. The mechanical instability of the electrode causes the transfer process to be difficult and a homogeneous

distribution of the electrode material is impossible. After the transfer process, the resulting MEA had several defects as some parts of the electrode were missing on the membrane. The MEAs produced by this technique are not suitable for reproducible measurements and will not be considered in the further diagnostics and serve as a strong motivation to change the coating process.

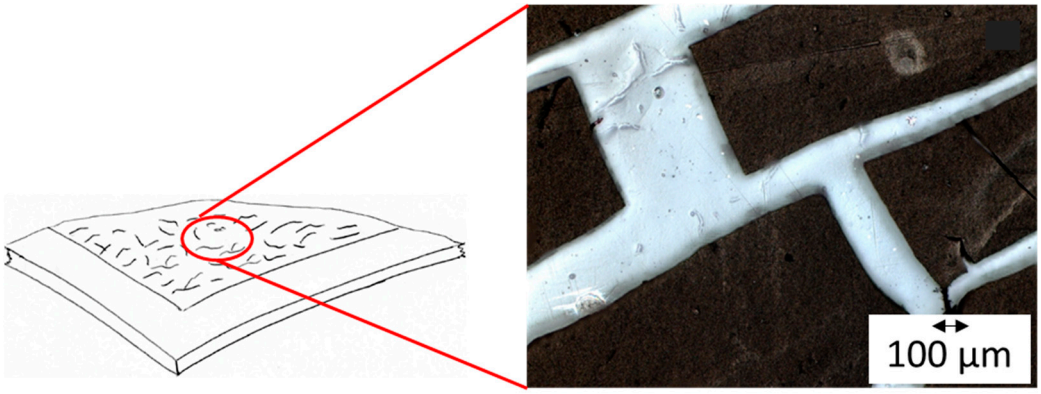

Figure 2. Optical microscopy image of a blade-coated electrode surface and its cracks caused channel widths after hot-pressing onto a Nafion® 115 membrane.

It is assumed that the drying procedures which were applied (RT and 60 °C) all yielded in an enrichment of water which, according to the previous results from our group, then caused a crack formation and the delamination of the electrode material [23]. The same study also shows that there are different critical crack thicknesses depending on the drying conditions. The thicker the layer (in our studies we used 80–268 µm) and the higher the surface tension at the end of the drying, the more cracks which occurred. As the necessary slot widths are all above the critical wet electrode thickness, this could be a potential reason for the formation of the cracks we have obtained in our MEA fabrication.

To examine this hypothesis, water was replaced by alcohols with higher boiling points. For that, 2-butanol (100 °C) and 1-pentanol (138 °C) were chosen. These inks resulted in relatively stable electrodes with cracks and no delamination that could easily be transferred to the membrane by hot-pressing. Accordingly, we assume that the critical crack thickness is still exceeded, but that there is no enrichment of water, which would lead to the delamination of the catalyst layer. Electrodes fabricated using inks based on 2-butanol und 1-pentanol were then used for performance testing. Figure 3 shows the polarization curves and power densities of a commercial DFMC MEA as a reference for comparing to MEAs with cathode doctor-blades coated using 2-butanol and 1-pentanol. The commercial MEA shows the highest performance. This is partially explained by the different catalyst loadings of our own MEAs in contrast to the commercial ones.

To minimize cracking, catalyst loadings were kept around at 0.4 mg cm^{-2}. Higher mass loadings, even with different solvents, also led to cracks and flake formations, just like with 2-propanol and water. Even if a water enrichment could possibly be excluded, our previous work showed that the formation of a crack above a critical thickness is totally depending on the layer thickness no matter if different temperatures or other drying parameters are chosen [40]. The catalyst loading of commercial catalysts is supposed to be around 1.5 mg cm^{-2}. Nevertheless, starting from 0.2 A cm^{-2}, in-house-produced MEAs show signs of mass transport limitations, leading to a steeper slope of the polarization curve. However, bearing in mind the significant difference in the mass loading, the PtNi-based electrodes already show potential for their use in fuel cell cathodes.

Even though our electrodes fabricated using 1-Pentanol show a promising performance already, cracking problems do not allow us to achieve the reproducibility of the electrode fabrication process and to increase the catalyst loading. This represents a problem which needs to be solved to conduct further measurements and characterizations with reproducible results.

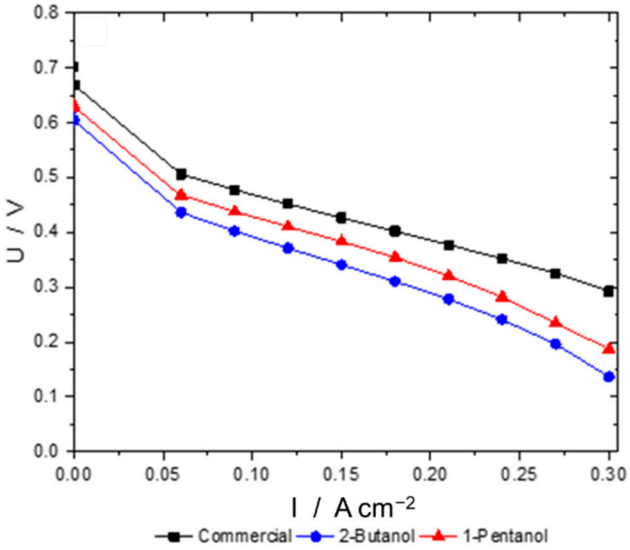

Figure 3. Polarization curves of a commercial MEA (1.5 mg cm^{-2}), an MEA with blade-coated electrode with 2-butanol (0.4 mg cm^{-2}) and an MEA with a blade-coated electrode with 1-pentanol (0.4 mg cm^{-2}). All with Nafion® 115 membranes. Operated with 0.8 mol L^{-1} methanol solution and 650 mL min^{-1} air at sea-level pressure.

As mentioned in the introductory part of this work ultrasonic spray deposition is another possibility to fabricate electrodes. As doctor-blade coating only allows for limited possibilities, the whole production method to fabricate MEAs was switched to ultrasonic spray deposition. The microscopic analysis was repeated with ultrasonically spray-deposited electrodes (Figure 4). The material distribution is much more homogeneous when compared to blade-coated electrodes and, in addition, no cracks are apparent. It is reported that if electrodes have an even distribution without cracks, they work as a local reinforcement for membranes [41]. In case of cracks within or the delamination of the catalyst layer, there is a loss of reinforcement, which enables a mechanical membrane failure. So, it is important to guarantee a full membrane coverage and an even distribution of the catalyst material to create a constant local reinforcement of the membrane and a uniform catalyst performance.

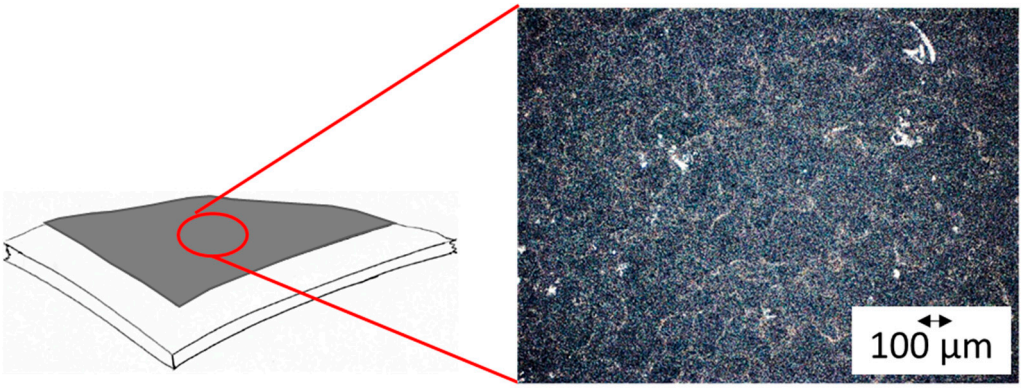

Figure 4. Optical microscopy image of an ultrasonically deposited electrode surface on a Nafion® 115 membrane.

We were able to confirm the even distribution of the catalyst material by performing a cross-section analysis of the MEAs using scanning electron microscopy (SEM) imaging. Figure 5a shows the catalyst-coated membrane by spray deposition. The thickness variation in the catalyst layer between maximum and minimum is around 2 µm. Another significant advantage is the better contact of the catalyst layer onto the membrane. In the spray-coated MEA, one can notice that the anode is fully in contact with the membrane. In

contrast, as marked on Figure 5b, the GDE anode does have complete contact with the membrane. In PEMFCs, it has been previously shown that a poor cathode–membrane interface leads to losses in the performance [42]. The unused MEA shown in Figure 5, which was hot-pressed onto the membrane, already shows some delamination at the blade-coated anode–membrane interphase (Figure 5b marked with a red circle). This result is confirmed by several other SEM images that are showing the same delamination areas.

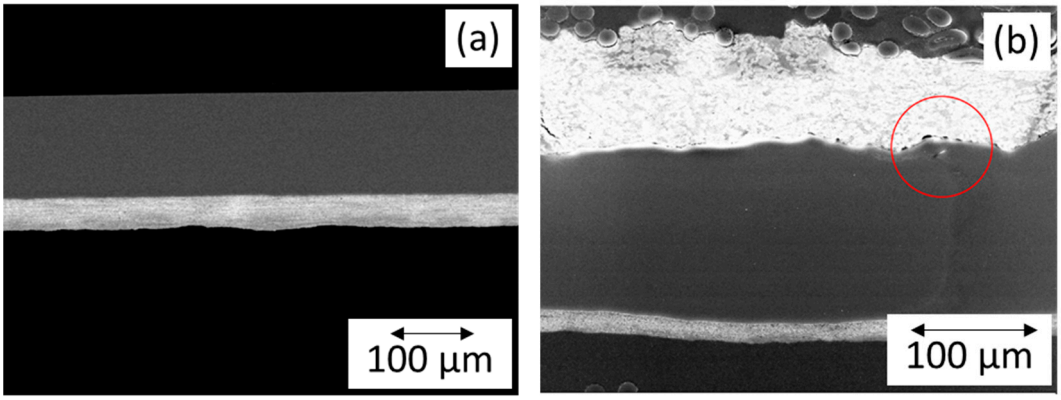

Figure 5. SEM images of a single-sided coated membrane (0.5 PtNi mg cm^{-2}) at the cathode (**a**) and MEA, including a GDL on the anode (upper-side), (**b**) with a delamination area marked by a red circle.

For directly spray-deposited electrodes, this problem seems to be negligible. In our experiments, none of the analyzed samples showed a delamination at the cathode–membrane interphase, even after having been operated for more than 1000 h. This challenge might also be negligible for thin catalyst layers. However, as the anode of a DMFC has a high catalyst loadings (up to 3 mg cm^{-2}) crack formation, deformations and a delamination along the membrane–electrode interface can be a problem.

3.2. Ink Preparation and Optimization of Spray-Coated Electrodes

Based on the previous results, the ongoing preparation is done exclusively by the ultrasonic spray deposition. For this process, different ink formulations were used to produce cathodes by coating the membrane with the catalyst material directly. Here, we predominantly examined three different aspects:

(a) The ionomer-to-carbon ratio (*I*/*C*);
(b) The water-to-propanol ratio (*W*/*P*);
(c) Catalyst loadings.

Figure 6a shows the polarization curves of MEAs with electrodes based on five different ionomer-to-carbon ratios, ranging from 0.4 to 0.87, and a constant water-to-propanol ratio (*W*/*P*) of 56/44. When analyzing the results in detail, it has to be considered that the operational average current density in a DMFC stack will be between 200 and 250 mA cm^{-2}. Thus, all further developments were focused on a maximum performance in that current density range. When looking at the polarization curves in Figure 6, there is an optimum range of the I/C ratios. Ratios of 0.87 and 0.77 both show mass transfer limitations at current densities starting from 160 mA cm^{-2} (*I*/*C* 0.87) or 180 mA cm^{-2} (*I*/*C* 0.77) as the slope begins to decrease nonlinearly. This indicates that under these conditions, too much ionomer is in the catalyst layer, resulting in the limitation of the oxygen and water mass transport in two possible ways:

1. Catalytically active sites are covered by the ionomer, leading to an inhomogeneous oxygen distribution within the catalyst layer [43].
2. As these ink formulations have high ionomer contents, they also bind permeated water and the water resulting from the oxygen reduction reaction to a higher degree, which leads to a detrimental water management at the micropores at the cathode electrode and, again, there is an inhomogeneous oxygen distribution within the electrode.

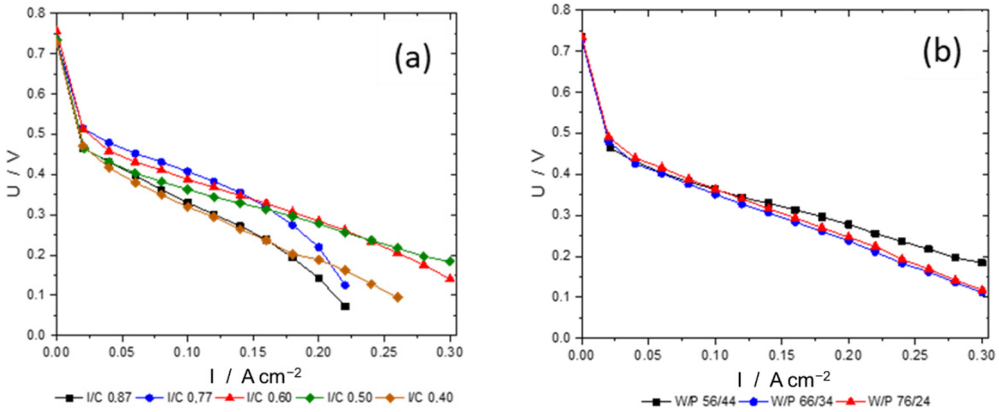

Figure 6. Polarization curves of MEAs with standard blade-coated anodes 3.0 $mg_{PtRu}cm^{-2}$ and cathodes 0.310–0.325 $mg_{PtNi}cm^{-2}$ produced by spray deposition. For all measurements Methanol concentration is const. 0.8 mol L^{-1} and air at sea level pressure is used. (**a**) cathodes with different ionomer-to-carbon ratios at constant *W/P* of 56/44; (**b**) cathodes with different water-to-propanol ratios with an ionomer-to-carbon ratio of 0.5.

Both aspects could be explanations for previously identified mass transport limitations. For an *I/C* of 0.4, the polarization curve has a much steeper slope in the ohmic region and the maximum power density is only 39 $mWcm^{-2}$ (except when compared with *I/C* 0.87). Here, it is likely that the amount of ionomer is too low and there is a low ionic conductivity, resulting in an inhomogeneous oxygen conversion this is the bottleneck of the electrochemical processes taking place in the cell. The optimum appears to be at the *I/C* ratios of 0.5 and 0.6, with a maximum power density of 57 $mWcm^{-2}$. Here, neither mass transfer limitations are reached within the examined current density range, nor are the ohmic losses as high as with *I/C* 0.4. Both values seem to be a good compromise between the need for a good ionic conductivity and the requirement for the high availability of the active sites. Later, these aspects shall be explained using electrochemical impedance spectroscopy. Thus, all further examinations were based on an *I/C* ratio of 0.5, as the polarization plots resulting from this preparation show stable cell voltages in the targeted current (200–250 mA cm^{-2}) regime.

When looking at different water-to-propanol ratios and the performances of the resulting electrodes within an MEA (Figure 6b), inks with *W/P* ratios of 66/34 or higher have higher ohmic losses and thus a steeper slope compared to the ratio of 56/44 [44]. So, the *W/P* ratio of 56/44 seems to represent an optimum and will be considered as the benchmark for the following analysis.

Cyclic voltammetry measurements were performed on the electrodes to analyze the underpotentially deposited hydrogen (H_{UPD}) peak (circled in red in Figure 7a), with them being integrated and used for ECSA calculations. In theory, the adsorption and desorption peaks have the same peak area. However, as shown in Figure 7a, it is difficult to determine where the adsorption peaks exactly start and end. Thus, in this work, only the desorption peak integrals were used for a further characterization. Figure 7 shows a typical CV diagram of one of the cathodes (a) and the peak area of the analysis (b).

For the reference charge, 210 µC cm^{-2} is used as it is the most common value for Pt catalysts [45,46]. However, our PtNi electrodes shall possess a Ni contribution to the ECSA, which means that using the value of 210 µC cm^{-2} leads to a systematic error with incorrect absolute surfaces. However, as the same material and batch is used for all ink compositions and the same procedure and calculation is applied at all measurements, it will not invalidate a direct comparison of the ECSA values of our cathodes to each other. Thus, these results should not be compared without a correction term to other catalyst materials such as pure platinum. The results of the CV measurements and ECSA calculations for different *I/C* and *W/P* ratios are summarized in Tables 1 and 2. Based on the developed reproducible catalyst materials and coating/processing techniques, we have now the option

to establish a data basis that will allow for the determination of correction terms that make these values comparable to platinum-based catalyst materials. This is ongoing research that will be presented later in an additional publication.

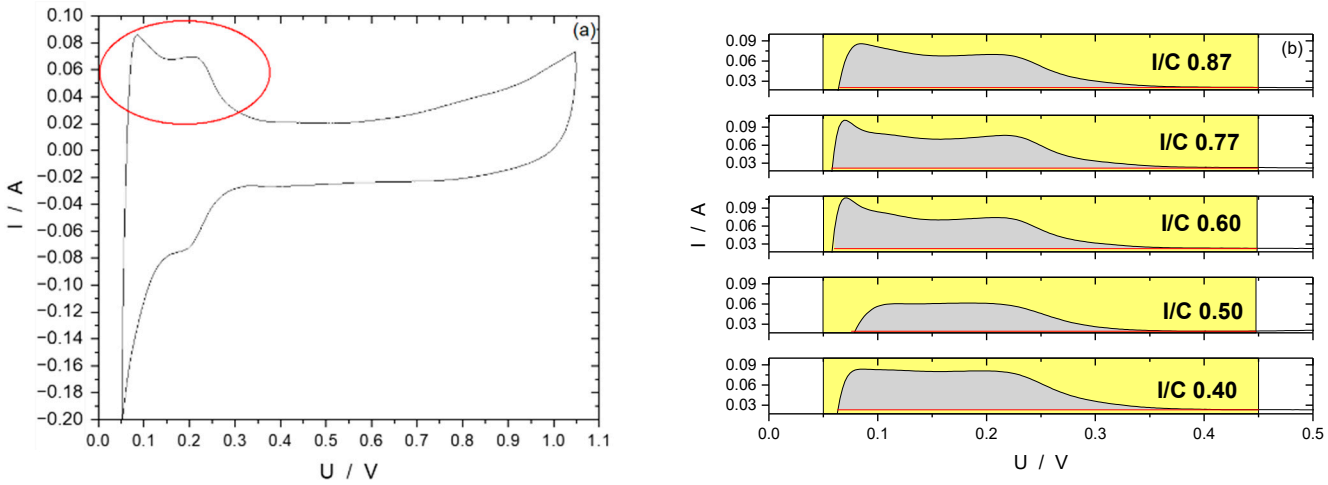

Figure 7. A representative CV diagram of a PtNi cathode (**a**) and a zoom-in and peak area analysis (**b**) of hydrogen desorption peaks with cathodes of different ionomer-to-carbon ratios from 0.87 to 0.4.

Table 1. ECSA values of spray-deposited PtNi-based cathodes with different *I/C* ratios (*W/P* ratio 56/44).

Ionomer-to-Carbon Ratio (*I/C*)	ECSA/m^2 g^{-1}
0.87	44.7
0.77	50.2
0.60	47.9
0.50	53.0
0.40	43.1

Table 2. ECSA values of spray-deposited PtNi-based cathodes with different *W/P* ratios (*I/C* ratio 0.5).

Water-to-Propanol Ratio (*W/P*)	ECSA/m^2 g^{-1}
56/44	**53.0**
66/34	45.6
76/24	46.4

The combination of *I/C* ratio: 0.5 and a *W/P* ratio: 56/44 shows the highest ECSA value compared to all other combinations. This result is in a good correlation with the first impression from the polarization measurements (Figure 6) as this combination of the production parameters also achieved the highest polarizations in the target current density area of 200–250 mA cm^{-2}. At this point, reference should be made once again to the previous publication of our group mentioned above, where it is shown that the proportion of nano-pores has an influence on the cell voltage; if too much Nafion® is used, it results in a blockage of these pores and parts of the catalyst particles no longer being supplied with air [22].

To gain further insights, EIS experiments were conducted. Since the catalyst material is utilized for ORR, it is necessary to determine the charge-transfer resistances R_{CT} of this specific reaction on this catalyst type to examine whether or not the ink formulation influences the charge-transfer resistances of the ORR. However, it is difficult to separate the impedance of a cathode when measuring in a single cell setup when both contributions for the anode and cathode simultaneously exist. Müller et al. were the first to develop a technique, starting with measuring the single cell impedance first, followed by a half-cell (anode) impedance measurement afterwards, and calculating the cathode impedance

by subtracting the anode impedance spectrum from the total cell spectrum finally [47]. Applying this technique not only gives an insight into the half-cell impedances of the cathode but also the half-cell potentials, which are shown in Figure 8 for different (a) *I/C* ratios and (b) *W/P* ratios. The half-cell potentials are plotted at different current densities and compared to the half-cell potentials of a commercial MEA. It is also obvious that the electrode with an *I/C* ratio of 0.87 underperforms compared to the other *I/C* ratios. This is confirmation of the poor performance of that specific MEA, as shown in Figure 6a, and is predominantly caused by the cathode. All other ratios result in more or less similar values in a corridor below the commercial electrode.

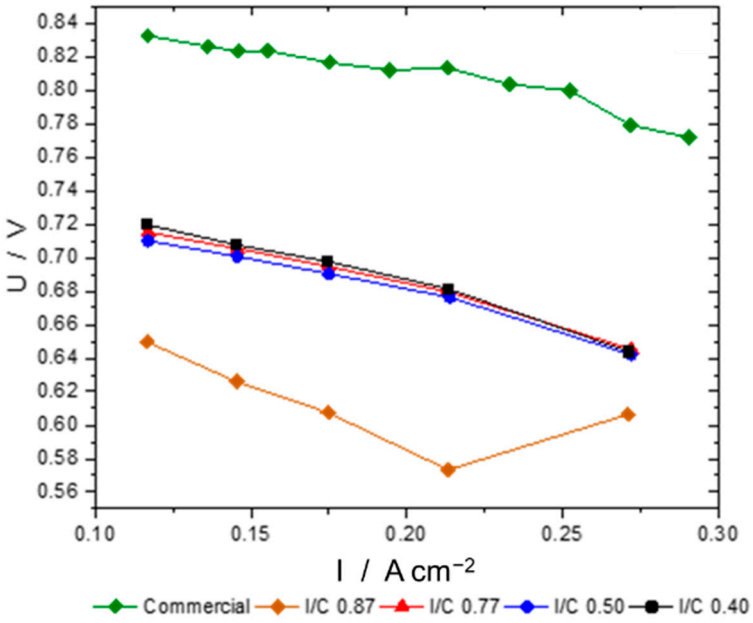

Figure 8. Half-cell potentials of cathodes with different *I/C* ratios.

For a further insight, the impedance spectra need to be analyzed in detail. Figure 9 shows the impedance spectra of the commercial MEA at different current densities (single-cell (a) and half-cell (b). The half-cell impedance spectrum (anode) is generated by purging the cathode with hydrogen during the half-cell measurement. This creates a Dynamic hydrogen electrode (DHE) on the cathode, where the protons from the anode are reduced, leading to a hydrogen evolution. It is assumed that the dynamic hydrogen electrode does not contribute to the measured impedances and all effects can be assigned to the anode [48].

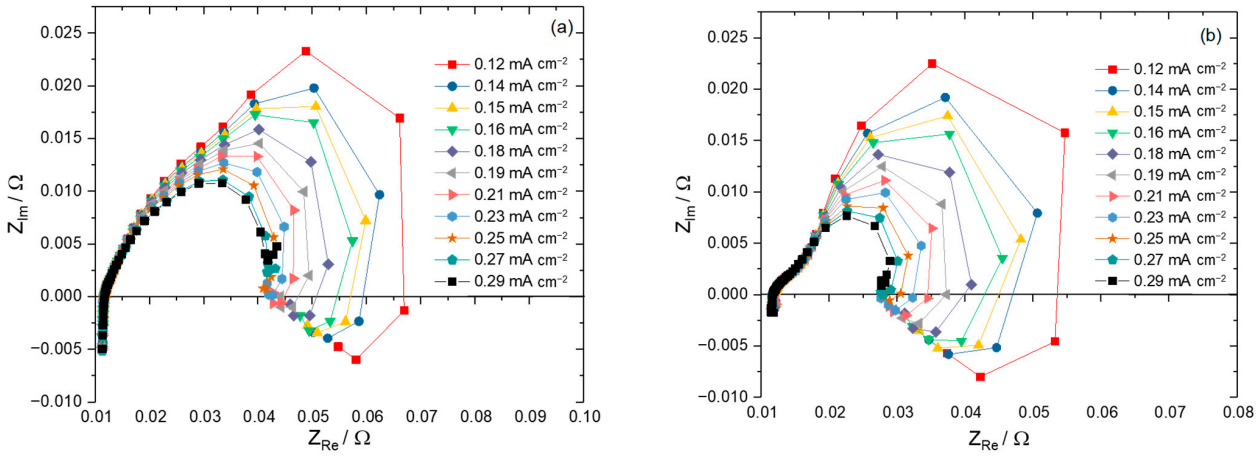

Figure 9. Single-cell (**a**) and half-cell [anode] (**b**) electrochemical impedance spectra of a commercial MEA at different current densities.

These spectra are subtracted (single-cell–half-cell [anode]) from each other and then fitted by simulation, as described in the experimental section. The resulting spectra show three different phase shifts (phase vs. frequency) and three different plateaus (|Z| vs. frequency) in a Bode plot (not shown here). Thus, we concluded that three different processes can be resolved. The first and second ones are possibly the oxygen reduction reaction and the oxidation of permeated methanol from the anode feed [49]. Even though a comparably high airflow rate of 650 mL min^{-1} was chosen, the third process is assumed to be the resistance caused by diffusion limitations, as it occurs at very low frequencies.

Wu et al. have proposed an equivalent circuit model (EEC) consisting of a series connection of an ohmic resistance and an RC combination (Randle EEC), representing a faradaic process without diffusion limitations [50]. Based on this, Du et al. used a general EEC with a series connection of an ohmic resistance and two R-C combinations representing a Faradaic impedance with two adsorbed species, as shown in Figure 10a. Here, the two adsorbed species are based on the oxygen reduction reaction (O_2H_{ads}) and methanol oxidation (CO_{ads}) from methanol that permeated from the anode. This model does not consider resistances by diffusion limitations but still represents the best experimental setup used in this work [51]. Nevertheless, in order to enhance that model and have a closer fit to our setup, it was modified in the following way:

1. In the case of this work, there is no ohmic resistance needed as all ohmic resistances (i.e., membrane, bipolar plates, endplates, etc.) are eliminated by the subtraction of anode half-cell impedances from single cell impedances.
2. In our measurements, a third phase shift was detected in the Bode plot, which was assumed to be a mass diffusion limitation.

Figure 10. Equivalent circuit models chosen for a DMFC cathode, with a series connection of an ohmic resistance and two R-C combinations representing a Faradaic impedance (**a**), with a series connection of three R-CPE elements, representing the ORR, methanol oxidation and mass transport limitations (**b**).

As there is no clear evidence that the assumption of a mass diffusion limitation is correct, instead of adding a Warburg element, we added another R-C combination to the model from Wu et al. Finally, instead of using capacitances, we replaced those by constant phase elements (CPE). The simulation results can give a hint to the type of resistance when analyzing the exponent of the CPE element. An exponent with values around 0 would be an ideal resistance, whereas values around 1 represent ideal capacitances. An exponent of 0.5 would be characteristic for diffusion-controlled processes. The resulting fit data all showed significances above zero which would be a first hint that the elements chosen for simulation are correlated to the processes occurring in the cell.

As an oxygen reduction reaction should be the most dominating of all the processes in the fuel cell cathode, it also has the biggest impact on the charge-transfer resistance. To identify the R-CPE combination representing the ORR, the pair with the largest charge-transfer resistance was chosen.

Further, the CPE element representing mass diffusion limitations (based on pre-experimental tests) usually has a magnitude of several hundred Farad. By searching for the combination of a CPE element with several hundred Farad and an exponent around 0.5, a CPE element representing a mass diffusion limitation can be identified. Lastly, the R-C combination that represents an oxygen reduction reaction is identified by looking for larger charge-transfer resistance values in combination with a CPE element that has an

exponent around one. Based on this, the last two datasets of the R-C combinations were analyzed and the results in Figure 11 show the values representing the charge-transfer resistances at different current densities, employing the model shown above. While the commercial cathode shows the lowest charge-transfer resistances, in-house electrodes have higher values. Here, the charge-transfer resistances for *I/C* 0.87 are the highest.

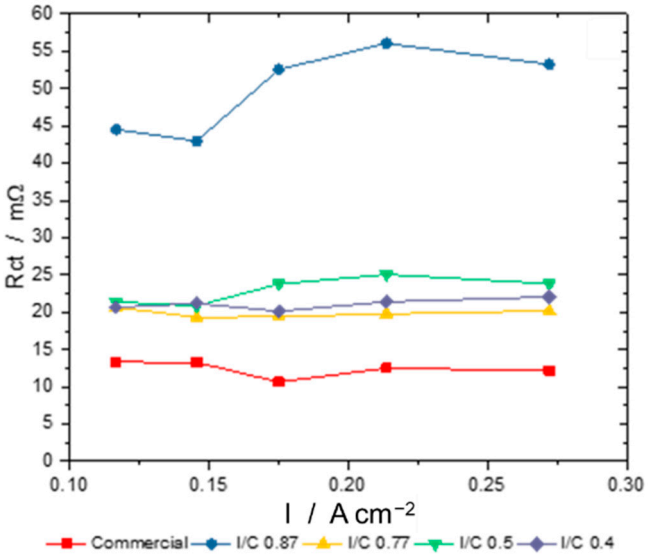

Figure 11. Charge-transfer resistances R_{CT} of electrodes with different *I/C* ratios.

As assumed earlier, based on the performance tests and ECSA calculations, the high ionomer content evidently causes a blocking of the catalyst's active sites and thus leads to an increase in the charge-transfer resistances during the oxygen reduction reaction. All other ink formulations, such as the *I/C* ratios of 0.77 to 0.4 and different *W/P* ratios from 56/44 to 76/24 and the commercial cathode, show a lower charge-transfer resistance.

3.3. Catalyst Loading

Based on these optimizations, different catalyst mass loadings were finally examined to determine an optimal catalyst amount. Here, the aim was to reach a high performance with the minimum possible amount of the catalyst. Figure 12 shows that catalyst loading should be designed based on the required operating conditions.

There are only small differences between the first three mass loadings, but it can be seen that the higher the loading, the better the performance. Only comparing the first three (0.325–0.695 mg cm^{-2}) to the highest mass loading shows a significant difference at the polarization and power density and a linear dependence of the power density and catalyst loading. Both findings are a clear indication of a well-designed electrode assembly that allows for the optimal performance of the cathode.

Even though values around or above 1 mg cm^{-2} seem quite high, DMFC cathodes need higher loadings compared to classic PEM fuel cells as catalyst poisoning due to the methanol permeation and oxidation of this permeating methanol at the cathode needs to be counteracted. This is the reason why the electrode with 1.13 mg cm^{-2} shows the highest polarization in the whole current density regime (Figure 12a), but its specific power in relation to catalyst loading is comparatively low (Figure 12b). Possibly, not all catalyst particles in the electrode layer are fully contributing to the ORR. The reason for this could be that some catalyst particles are not properly connected to the electrode's structure, or the catalyst particles are not in contact with oxygen. This behavior is likely to be strengthened by the increased thickness of the catalyst layer with a higher loading. The increased thickness leads to a higher resistivity due to the increased length of the ionic conductive phase and, additionally, the mass transport of oxygen and water and water vapor is impeded in the thicker layers.

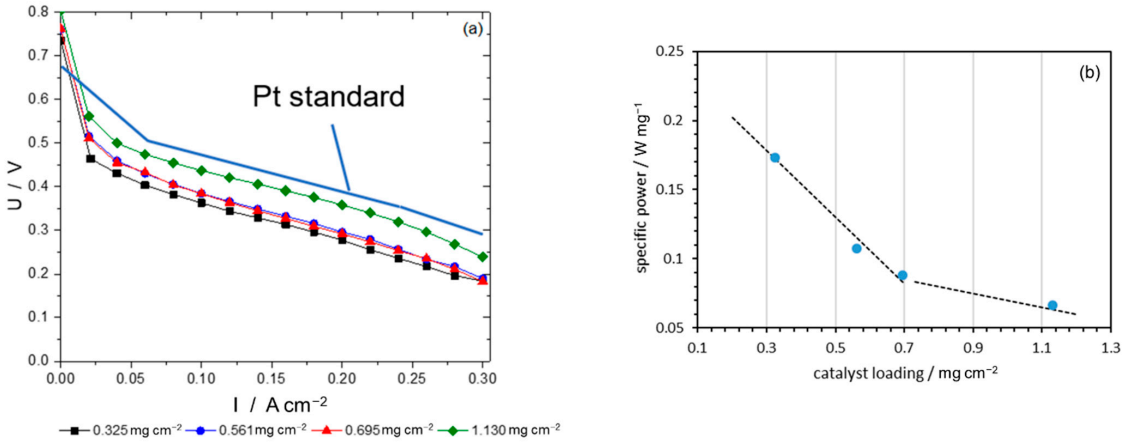

Figure 12. Polarization curves of MEAs with spray-deposited cathodes of different loadings with *I/C* of 0.5 and *W/P* of 56/44 (Methanol 0.8 mol L^{-1}; sea level pressure; anode 3.0 mg cm^{-1} PtRu), Pt standard MEA with ~1.5 mg/cm^2 see also Figure 3 (**a**), specific power in W mg^{-1} catalyst over the catalyst loading in mg cm^{-2} at 225 mA/cm^2 (**b**).

4. Conclusions

The proper design of ink compositions for the coating of electrochemical electrodes for fuel cells is essential to achieve high polarizations at the whole current density range. The aim in the cathode's development, especially for DMFCs, is to achieve high exchange current densities and, additionally, high conversion rates for the permeating methanol. These are reasons for using catalyst loadings of about 1 mg/cm^2 or more. At such loadings, thick catalyst layers (~200 µm) are necessary. The formation of cracks in the electrode during the drying can easily occur and must be prevented to ensure a high lateral conductivity. However, this is only possible to a limited extent when using doctor blade coatings, even when the solvents were adapted and therefore the coating in the described characterizations was done by ultrasonic spray deposition.

In this work, the parameters' ionomer-to-carbon ratio (*I/C*), water-to-propanol ratio (*W/P*), and catalyst loading were varied. It was found that especially the ionomer-to-carbon ratio *I/C* had a significant influence on the electrode's performance, while the influence of the water-to-propanol ratio *W/P* was much smaller. In this work the best performance was achieved with *I/C* = 0.6 for current densities close to 0.2 A cm^{-2}. For lower current densities (0.1 A cm^{-2}), a higher *I/C* (0.77) was better, whereas for higher current densities (0.3 A cm^{-2}), a lower *I/C* of 0.5 lead to a better performance.

The electrochemical active surface area was highest for the intermediate *I/C* = 0.5. The specific power per amount of catalyst [W/mg$_{PtNi}$] decreased linearly with increasing catalyst loading in DMFCs for catalyst loadings in the range 0.3–1 mg cm^{-2}, starting from 0.175 W mg^{-1} with a slope of about −0.2 W cm^2 mg^{-2}. At catalyst loadings above 1 mg cm^{-2}, the curve of a specific power is flatter. This indicates that at catalyst loadings beyond 1 mg cm^{-2}, while still contributing to the cell performance, the catalyst was not fully used.

The effect of the electrode's composition on the charge-transfer resistance, as determined by electrochemical impedance spectroscopy, is rather small. Only for extreme values of I/C (0.4 or 0.87) is a significant increased charge-transfer resistance observed, which is affected by an unsuitable integration into the electrode matrix. As a result, we assume that the catalyst layer composition now is close to the best possible performance of the electrodes.

For further improvements, high-quality Ni-Pt core–shell particles could especially help to increase performances and decrease resistances while keeping the catalyst loadings to a minimum. With a reliable source of high-quality nanoparticle catalyst material manufactured by a flow reactor at the gram scale, further studies with regard to the optimal operating parameters and catalyst loadings in DMFCs are easily possible as the results will be compatible and reproducible.

Author Contributions: Writing—original draft, A.K.; Writing—review & editing, A.G., K.W., S.M., A.C.Y.-N., S.W., C.G., M.M., G.B., H.W. and M.C.; Supervision, D.S. All authors have read and agreed to the published version of the manuscript.

Funding: This research was funded by the Bundesministerium für Wirtschaft und Energie within the HiKAB Project [03ET1435A-C]. This work was authored in part by the National Renewable Energy Laboratory, operated by the Alliance for Sustainable Energy, LLC, for the U.S. Department of Energy (DOE) under Contract No. [DE-AC36-08GO28308]. Funding was provided by the U.S. Department of Energy Office of Energy Efficiency and Renewable Energy (EERE) Hydrogen and Fuel Cell Technologies Office (HFTO), Award No. [DE-EE0008836]. The views expressed in the article do not necessarily represent the views of the DOE or the U.S. Government. The publisher, by accepting the article for publication, acknowledges that the U.S. Government retains a nonexclusive, paid-up, irrevocable, worldwide license to publish or reproduce the published form of this work, or allow others to do so, for U.S. Government purposes. The publication is also funded by the Deutsche Forschungsgemeinschaft (DFG, German Research Foundation) [491111487].

Data Availability Statement: Data is contained within the article.

Acknowledgments: We would like to thank the hydrogen and fuel cell center ZBT GmbH for carrying out the initial ultrasonic spray deposition experiments and processing our catalyst powders to the electrodes. Finally, we would like to thank everyone who supported this work in the laboratory or contributed to the success of this work in various discussions.

Conflicts of Interest: The authors declare no conflict of interest.

Glossary

List of Symbols

A_{PI}	Peak integral
ν	Scan rate
Q	Charge density
M_{PtNi}	Mass loading of PtNi catalyst
A_{Geo}	Geometric area of the electrode
H_{UPD}	Underpotentially deposited hydrogen
R_{CT}	Charge-transfer resistance
I/C	Ionomer-to-carbon ratio
W/P	Water-to-propanol ratio

List of Acronyms

CPE	Constant phase elements
CV	Cyclic voltammetry
DFT	Density functional theory
DHE	Dynamic hydrogen electrode
DMFC	Direct methanol fuel cell
ECSA	Electrochemically active surface area
EDX	Energy-dispersive X-ray spectroscopy
EEC	Equivalent electrical circuit
EIS	Electrochemical impedance spectroscopy
GDE	Gas diffusion electrode
GDL	Gas diffusion layer
IEA	International Energy Agency
MEA	Membrane electrode assembly
ORR	Oxygen reduction reaction
PEM	Proton electrolyte membrane
PEMFC	Polymer electrolyte membrane fuel cell
RHE	Reversible hydrogen electrode
RT	Room temperature (~25 °C)
SEM	Scanning electron microscopy
TEM	Transmission electron microscopy
XPS	X-ray photoelectron spectroscopy

References

1. Agency, I.E. *World Energy Outlook*; OECD: Paris, France, 2004.
2. Finanzen.net—Platinpreis. Available online: https://www.finanzen.net/rohstoffe/platinpreis (accessed on 20 July 2021).
3. Bashyam, R.; Zelenay, P. A class of non-precious metal composite catalysts for fuel cells. In *Materials for Sustainable Energy: A Collection of Peer-Reviewed Research and Review Articles from Nature Publishing Group*; World Scientific: Singapore, 2011; pp. 247–250.
4. Othman, R.; Dicks, A.L.; Zhu, Z. Non precious metal catalysts for the PEM fuel cell cathode. *Int. J. Hydrog. Energy* **2012**, *37*, 357–372. [CrossRef]
5. Banham, D.; Ye, S.; Pei, K.; Ozaki, J.-I.; Kishimoto, T.; Imashiro, Y. A review of the stability and durability of non-precious metal catalysts for the oxygen reduction reaction in proton exchange membrane fuel cells. *J. Power Sources* **2015**, *285*, 334–348. [CrossRef]
6. Martinaiou, I.; Monteverde Videla, A.H.A.; Weidler, N.; Kübler, M.; Wallace, W.D.Z.; Paul, S.; Wagner, S.; Shahraei, A.; Stark, R.W.; Specchia, S.; et al. Activity and degradation study of an Fe-N-C catalyst for ORR in Direct Methanol Fuel Cell (DMFC). *Appl. Catal. B Environ.* **2020**, *262*, 118217. [CrossRef]
7. de Sá, M.H.; Moreira, C.S.; Pinto, A.M.F.R.; Oliveira, V.B. Recent Advances in the Development of Nanocatalysts for Direct Methanol Fuel Cells. *Energies* **2022**, *15*, 6335. [CrossRef]
8. Ulas, B.; Yagizatli, Y.; Demir-Kivrak, H. 3—Metal-free catalysts for fuel cell applications. In *Carbon-Based Metal Free Catalysts*; Asiri, A.M.A., Khan, A., Bhawani, S.A., Abu-Zied, B.M.M., Siengchin, S., Džudžević-Čančar, H., Eds.; Elsevier: Amsterdam, The Netherlands, 2022; pp. 67–109.
9. Lo Vecchio, C.; Serov, A.; Dicome, M.; Zulevi, B.; Aricò, A.S.; Baglio, V. Investigating the durability of a direct methanol fuel cell equipped with commercial Platinum Group Metal-free cathodic electro-catalysts. *Electrochim. Acta* **2021**, *394*, 139108. [CrossRef]
10. Shi, J.; Shao, H.; Yang, F.; Li, J.; Fan, L.; Cai, W. Dual-template induced multi-scale porous Fe@FeNC oxygen reduction catalyst for high-performance electrochemical devices. *Chem. Eng. J.* **2022**, *445*, 136628. [CrossRef]
11. Thiagarajan, V.; Karthikeyan, P.; Thanarajan, K.; Neelakrishnan, S.; Manoharan, R.; Chen, R.; Fly, A.; Anand, R.; Karuppa Raj, T.R.; Sendhil Kumar, N. Experimental investigation on DMFCs using reduced noble metal loading with NiTiO3 as supportive material to enhance cell performances. *Int. J. Hydrog. Energy* **2019**, *44*, 13415–13423. [CrossRef]
12. Kaur, A.; Kaur, G.; Singh, P.P.; Kaushal, S. Supported bimetallic nanoparticles as anode catalysts for direct methanol fuel cells: A review. *Int. J. Hydrog. Energy* **2021**, *46*, 15820–15849. [CrossRef]
13. Mansor, M.; Timmiati, S.N.; Lim, K.L.; Wong, W.Y.; Kamarudin, S.K.; Nazirah Kamarudin, N.H. Recent progress of anode catalysts and their support materials for methanol electrooxidation reaction. *Int. J. Hydrog. Energy* **2019**, *44*, 14744–14769. [CrossRef]
14. Wang, C.; Chi, M.; Wang, G.; Van der Vliet, D.; Li, D.; More, K.; Wang, H.H.; Schlueter, J.A.; Markovic, N.M.; Stamenkovic, V.R. Correlation between Surface Chemistry and Electrocatalytic Properties of Monodisperse PtxNi1-x Nanoparticles. *Adv. Funct. Mater.* **2011**, *21*, 147–152. [CrossRef]
15. Stamenkovic, V.; Mun, B.S.; Mayrhofer, K.J.; Ross, P.N.; Markovic, N.M.; Rossmeisl, J.; Greeley, J.; Nørskov, J.K. Changing the activity of electrocatalysts for oxygen reduction by tuning the surface electronic structure. *Angew. Chem. Int. Ed.* **2006**, *45*, 2897–2901. [CrossRef] [PubMed]
16. Antolini, E.; Salgado, J.; Gonzalez, E. Carbon supported Pt75M25 (M= Co, Ni) alloys as anode and cathode electrocatalysts for direct methanol fuel cells. *J. Electroanal. Chem.* **2005**, *580*, 145–154. [CrossRef]
17. Toda, T.; Igarashi, H.; Uchida, H.; Watanabe, M. Enhancement of the electroreduction of oxygen on Pt alloys with Fe, Ni, and Co. *J. Electrochem. Soc.* **1999**, *146*, 3750–3756. [CrossRef]
18. Glüsen, A.; Dionigi, F.; Paciok, P.; Heggen, M.; Müller, M.; Gan, L.; Strasser, P.; Dunin-Borkowski, R.E.; Stolten, D. Dealloyed PtNi-Core–Shell Nanocatalysts Enable Significant Lowering of Pt Electrode Content in Direct Methanol Fuel Cells. *ACS Catal.* **2019**, *9*, 3764–3772. [CrossRef]
19. Subbaraman, R.; Strmcnik, D.; Paulikas, A.P.; Stamenkovic, V.R.; Markovic, N.M. Oxygen Reduction Reaction at Three-Phase Interfaces. *ChemPhysChem* **2010**, *11*, 2825–2833. [CrossRef]
20. Andersen, S.M.; Grahl-Madsen, L. Interface contribution to the electrode performance of proton exchange membrane fuel cells–Impact of the ionomer. *Int. J. Hydrog. Energy* **2016**, *41*, 1892–1901. [CrossRef]
21. Antolini, E.; Giorgi, L.; Pozio, A.; Passalacqua, E. Influence of Nafion loading in the catalyst layer of gas-diffusion electrodes for PEFC. *J. Power Sources* **1999**, *77*, 136–142. [CrossRef]
22. Glüsen, A.; Müller, M.; Stolten, D. The Effect of Nafion Content on DMFC Electrode Characteristics. *ECS Trans.* **2013**, *58*, 1023–1029. [CrossRef]
23. Scheepers, F.; Stähler, A.; Stähler, M.; Carmo, M.; Lehnert, W.; Stolten, D. Steering and in situ monitoring of drying phenomena during film fabrication. *J. Coat. Technol. Res.* **2019**, *16*, 1213–1221. [CrossRef]
24. Shang, Z.; Hossain, M.M.; Wycisk, R.; Pintauro, P.N. Poly(phenylene sulfonic acid)-expanded polytetrafluoroethylene composite membrane for low relative humidity operation in hydrogen fuel cells. *J. Power Sources* **2022**, *535*, 231375. [CrossRef]
25. Mao, Q.; Sun, G.; Wang, S.; Sun, H.; Wang, G.; Gao, Y.; Ye, A.; Tian, Y.; Xin, Q. Comparative studies of configurations and preparation methods for direct methanol fuel cell electrodes. *Electrochim. Acta* **2007**, *52*, 6763–6770. [CrossRef]
26. Park, I.-S.; Li, W.; Manthiram, A. Fabrication of catalyst-coated membrane-electrode assemblies by doctor blade method and their performance in fuel cells. *J. Power Sources* **2010**, *195*, 7078–7082. [CrossRef]

27. Rohendi, D.; Syarif, N.; Said, M.; Utami, M.T.; Marcelina, Y. Utilization of catalyst-coated membrane (CCM) and spraying methods in fabrication membrane electrode assembly (MEA) for direct methanol fuel Cell (DMFC) using Pt-Co/C catalyst. *J. Phys. Conf. Ser.* **2019**, *1282*, 012065. [CrossRef]
28. Moganapriya, C.; Rajasekar, R.; Gobinath, V.K.; Mohankumar, A. Fabrication and Properties of the Polymer Electrolyte Membrane (PEM) for Direct Methanol Fuel Cell Applications. In *Nanomaterials for Alcohol Fuel Cells*; Inamuddin, Rangreez, T.A., Sen, F., Asiri, A.M., Eds.; Materials Research Forum LLC: Millersville, PA, USA, 2019; Volume 49, pp. 164–166.
29. Engle, R. Maximizing the Use of Platinum Catalyst by Ultrasonic Spray Application. *J. Fuel Cell Sci. Technol.* **2012**, *9*, 014501-1–014501-7. [CrossRef]
30. Zainoodin, A.M.; Tsujiguchi, T.; Masdar, M.S.; Kamarudin, S.K.; Osaka, Y.; Kodama, A. Performance of a direct formic acid fuel cell fabricated by ultrasonic spraying. *Int. J. Hydrog. Energy* **2018**, *43*, 6413–6420. [CrossRef]
31. Yang, Y.J.; Li, W. Ultrasonic assisted coating of multiwalled carbon nanotubes with NiFe-layered double hydroxide for improved electrocatalytic oxygen reduction. *J. Electroanal. Chem.* **2018**, *823*, 499–504. [CrossRef]
32. Stähler, M.; Stähler, A.; Scheepers, F.; Carmo, M.; Stolten, D. A completely slot die coated membrane electrode assembly. *Int. J. Hydrog. Energy* **2019**, *44*, 7053–7058. [CrossRef]
33. Stähler, A.; Stähler, M.; Scheepers, F.; Carmo, M.; Stolten, D. Reusability of decal substrates for the fabrication of catalyst coated membranes. *Int. J. Adhes. Adhes.* **2020**, *98*, 102473. [CrossRef]
34. Sharma, J.; Lyu, X.; Reshetenko, T.; Polizos, G.; Livingston, K.; Li, J.; Wood, D.L.; Serov, A. Catalyst layer formulations for slot-die coating of PEM fuel cell electrodes. *Int. J. Hydrog. Energy* **2022**, *47*, 35838–35850. [CrossRef]
35. Glüsen, A.; Müller, M.; Kimiaie, N.; Konradi, I.; Mergel, J.; Stolten, D. Manufacturing Technologies for Direct Methanol Fuel Cells (DMFCs). In *18th World Hydrogen Energy Conference 2010—WHEC 2010 proceedings*; Detlef Stolten, T.G.E., Ed.; Parallel Sessions Book 1: Fuel Cell Basics/Fuel Infrastructures; Forschungszentrum Jülich GmbH: Jülich, Germany, 2010; Volume 78-1, pp. 219–226.
36. Ahrenstorf, K.; Albrecht, O.; Heller, H.; Kornowski, A.; Görlitz, D.; Weller, H. Colloidal synthesis of NixPt1− x nanoparticles with tuneable composition and size. *Small* **2007**, *3*, 271–274. [CrossRef]
37. Lim, B.H.; Majlan, E.H.; Tajuddin, A.; Husaini, T.; Wan Daud, W.R.; Mohd Radzuan, N.A.; Haque, M.A. Comparison of catalyst-coated membranes and catalyst-coated substrate for PEMFC membrane electrode assembly: A review. *Chin. J. Chem. Eng.* **2021**, *33*, 1–16. [CrossRef]
38. Cooperation, S.T. Ultrasonic Atomization. Available online: https://www.sono-tek.com/ultrasonic-coating/how-ultrasonic-nozzles-work/ (accessed on 30 December 2022).
39. Glüsen, A.; Müller, M.; Stolten, D. 45% Cell Efficiency in DMFCs via Process Engineering. *Fuel Cells* **2020**, *20*, 507–514. [CrossRef]
40. Scheepers, F.; Stähler, A.; Stähler, M.; Carmo, M.; Lehnert, W.; Stolten, D. Layer Formation from Polymer Carbon-Black Dispersions. *Coatings* **2018**, *8*, 450. [CrossRef]
41. Singh, Y.; White, R.T.; Najm, M.; Haddow, T.; Pan, V.; Orfino, F.P.; Dutta, M.; Kjeang, E. Tracking the evolution of mechanical degradation in fuel cell membranes using 4D in situ visualization. *J. Power Sources* **2019**, *412*, 224–237. [CrossRef]
42. Mauger, S.A.; Pfeilsticker, J.R.; Wang, M.; Medina, S.; Yang-Neyerlin, A.C.; Neyerlin, K.C.; Stetson, C.; Pylypenko, S.; Ulsh, M. Fabrication of high-performance gas-diffusion-electrode based membrane-electrode assemblies. *J. Power Sources* **2020**, *450*, 227581. [CrossRef]
43. Pickup, P.G.; Li, G. Ionic Conductivity of PEMFC Electrodes: Effect of Nafion Loading. *J. Electrochem. Soc.* **2003**, *150*, C745–C752.
44. Van Cleve, T.; Khandavalli, S.; Chowdhury, A.; Medina, S.; Pylypenko, S.; Wang, M.; More, K.L.; Kariuki, N.; Myers, D.J.; Weber, A.Z.; et al. Dictating Pt-Based Electrocatalyst Performance in Polymer Electrolyte Fuel Cells, from Formulation to Application. *ACS Appl. Mater. Interfaces* **2019**, *11*, 46953–46964. [CrossRef]
45. Moniri, S.; Van Cleve, T.; Linic, S. Pitfalls and best practices in measurements of the electrochemical surface area of platinum-based nanostructured electro-catalysts. *J. Catal.* **2017**, *345*, 1–10. [CrossRef]
46. Shao, M.; Odell, J.H.; Choi, S.-I.; Xia, Y. Electrochemical surface area measurements of platinum-and palladium-based nanoparticles. *Electrochem. Commun.* **2013**, *31*, 46–48. [CrossRef]
47. Müller, J.T.; Urban, P.M.; Hölderich, W.F. Impedance studies on direct methanol fuel cell anodes. *J. Power Sources* **1999**, *84*, 157–160. [CrossRef]
48. Springer, T.; Zawodzinski, T.; Wilson, M.; Gottesfeld, S. Characterization of polymer electrolyte fuel cells using AC impedance spectroscopy. *J. Electrochem. Soc.* **1996**, *143*, 587–599. [CrossRef]
49. Du, C.; Zhao, T.; Xu, C. Simultaneous oxygen-reduction and methanol-oxidation reactions at the cathode of a DMFC: A model-based electrochemical impedance spectroscopy study. *J. Power Sources* **2007**, *167*, 265–271. [CrossRef]
50. Wu, X.; Ma, H.; Chen, S.; Xu, Z.; Sui, A. General equivalent circuits for faradaic electrode processes under electrochemical reaction control. *J. Electrochem. Soc.* **1999**, *146*, 1847–1853. [CrossRef]
51. Furukawa, K.; Okajima, K.; Sudoh, M. Structural control and impedance analysis of cathode for direct methanol fuel cell. *J. Power Sources* **2005**, *139*, 9–14. [CrossRef]